Key issues of ultraviolet radiation of OH at high altitudes

Yuhuai Zhang, Tian Wan, Jianzheng Jiang, and Jing Fan

Citation: AIP Conference Proceedings **1628**, 1168 (2014); doi: 10.1063/1.4902725
View online: http://dx.doi.org/10.1063/1.4902725
View Table of Contents: http://scitation.aip.org/content/aip/proceeding/aipcp/1628?ver=pdfcov
Published by the AIP Publishing

Key Issues of Ultraviolet Radiation of OH at High Altitudes

Yuhuai Zhang, Tian Wan, Jianzheng Jiang and Jing Fan

State Key Laboratory of High Temperature Gasdynamics, Institute of Mechanics, Chinese Academy of Sciences, Beijing 100190, China

Abstract. Ultraviolet (UV) emissions radiated by hydroxyl (OH) is one of the fundamental elements in the prediction of radiation signature of high-altitude and high-speed vehicle. In this work, the OH $A^2\sum^+ \rightarrow X^2\prod$ ultraviolet emission band behind the bow shock is computed under the experimental condition of the second bow-shock ultraviolet flight (BSUV-2). Four related key issues are discussed, namely, the source of hydrogen element in the high-altitude atmosphere, the formation mechanism of OH species, efficient computational algorithm of trace species in rarefied flows, and accurate calculation of OH emission spectra. Firstly, by analyzing the typical atmospheric model, the vertical distributions of the number densities of different species containing hydrogen element are given. According to the different dominating species containing hydrogen element, the atmosphere is divided into three zones, and the formation mechanism of OH species is analyzed in the different zones. The direct simulation Monte Carlo (DSMC) method and the Navier-Stokes equations are employed to compute the number densities of the different OH electronically and vibrationally excited states. Different to the previous work, the trace species separation (TSS) algorithm is applied twice in order to accurately calculate the densities of OH species and its excited states. Using a non-equilibrium radiation model, the OH ultraviolet emission spectra and intensity at different altitudes are computed, and good agreement is obtained with the flight measured data.

Keywords: hypersonic reentry, rarefied gas flow, bow-shock, ultraviolet radiation, hydroxyl.
PACS: 47.45.-n, 78.20.Bh.

ATMOSPHERIC MODEL AT HIGH ALTITUDE

Ultraviolet emission is very important for radiation signature of hypersonic vehicles at high altitude. In the early 90s last century, bow-shock ultraviolet flight experiments (BSUV) [1, 2] was conducted in the United States. During the experiments, radiation intensity of the flow field was measured by onboard spectrometers and photometers. The experiment has been numerically simulated by many researchers [3-6]. For example, the hydroxyl (OH) emission intensity computed by Boyd et al. [5] was lower than the measured data by more than one magnitude. By increasing the free-stream OH mole fraction by 20 times, the re-computed intensity agreed with the experiment.

However, the atmosphere composition has its regular pattern. Figure 1 plots the number density of major species containing hydrogen-element at different altitudes [7]. It shows that OH is relatively small in comparison with other species containing hydrogen-element, and therefore OH behind the bow shock may not originate from the free-stream. From the distribution of the species, the atmosphere can be divided into three zones: zone 1 covers altitude below 75 km, where the major source of hydrogen-element is from H_2O; zone 2 covers altitude between 75 km and 85 km, where the major source of hydrogen-element is from H_2O, H_2 and H; zone 3 covers altitude above 85 km, where the major source of hydrogen-element is from H_2 and H. The altitude of interest in this work is between 80 km and 100 km, which belong to zone 2 and zone 3.

HYDROXYL RADICAL FORMATION REACTIONS

To correctly calculate the OH number density behind bow shock, the selection of OH formation reactions and their rate coefficient evaluation is critical. Table 1 lists the key reactions relevant to OH formation. The rate coefficients of reactions 1-4 and 5-6 are taken from Gimelshein et al. [8] and Shatalov et al. [9], respectively. The formation mechanism of OH can be divided into three categories: the first mechanism is dissociation reaction of H_2O (reactions 1, 2 and 3); the second is exchange reaction of H atom (reaction 4); the third is exchange reaction of H_2 molecule (reactions 5 and 6).

Proceedings of the 29th International Symposium on Rarefied Gas Dynamics
AIP Conf. Proc. 1628, 1168-1175 (2014); doi: 10.1063/1.4902725

TABLE 1. Key reactions relevant to OH formation.

No.	Reaction	Rate Coefficient (m-molecule-s)	Source
1	$H_2O+N_2 \rightarrow OH+H+N_2$	$5.81\times10^{-15}\exp(-53000/T)$	Gimelshein (2003) [8]
2	$H_2O+M \rightarrow OH+H+M$ (M=O, O_2)	$1.13\times10^{-7}T^{-1.31}\exp(-59400/T)$	Gimelshein (2003)
3	$O+H_2O \rightarrow OH+OH$	$1.13\times10^{-16}\exp(-9240/T)$	Gimelshein (2003)
4	$H+O_2 \rightarrow OH+O$	$1.66\times10^{-16}\exp(-7690/T)$	Gimelshein (2003)
5	$H_2+O \rightarrow OH+H$	$8.47\times10^{-26}\ T^{2.67}\exp(-3165/T)$	Shatalov (2009) [9]
6	$H_2+O_2 \rightarrow OH+OH$	$2.82\times10^{-17}\exp(-24044/T)$	Shatalov (2009)

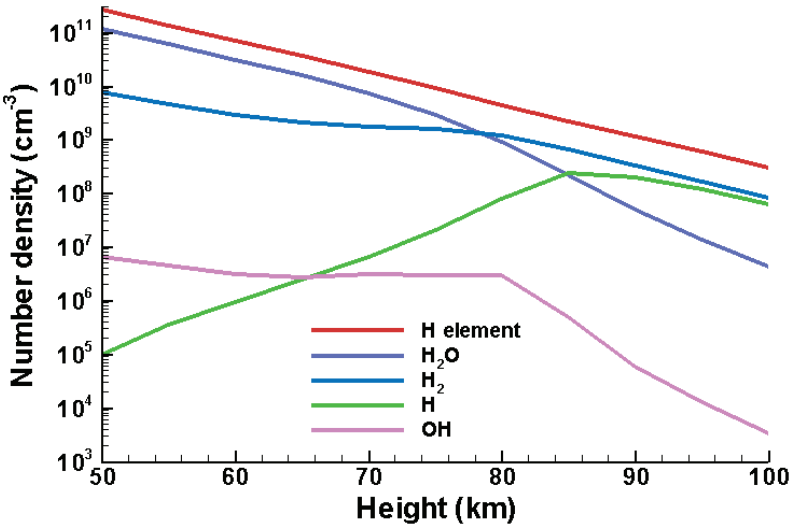

FIGURE 1. Number density of major species containing hydrogen-element at different altitudes.

In zone 1 defined in the foregoing section where the major source of hydrogen-element is from H_2O, the formation of OH is from reactions 1, 2 and 3; in zone 2 where the major source of hydrogen-element is from H_2O, H_2 and H, the formation of OH is from reactions 1 to 6; in zone 3 where the major source of hydrogen-element is from H_2 and H, the formation of OH is from reactions 4 to 6. Note that Gimelshein et al. [8] analyzed the OH formation mechanism versus the altitude and drew a similar conclusion. In this work, we point out that the difference in the free-stream condition is the driving force that causes the difference in the OH formation mechanism.

COMPUTATIONAL METHODS

The DSMC method and the compressible Navier-Stokes equations are both applied for simulating the second flight experiment of bow shock ultraviolet (BSUV-2). For hydroxyl emission interested here, a chemical reaction model of 12 species is employed that includes N_2, N, O_2, O, and NO; H_2O, OH, H_2 and H; electronically and vibrationally excited states OH (A; v'=0; 1; 2). The reaction rates for the five-species air (N_2, N, O_2, O, NO) come from the database compiled by Bortner [10]; those for the hydrogenated species are taken from [8, 9], and the excitation and quenching coefficient rates are from [5]. For the reactions of five-species air, the Variable Hard Sphere (VHS) model is used for the molecular collision potential, the Larsen-Borgnakke (LB) model (Z_R = 5, Z_V = 50) is employed in the rotational and vibrational internal energy exchanges, the total collision energy (TEC) model [11] is used for chemical reactions. The accommodation coefficients of the translational, rotational and vibrational modes were set to 1.0, respectively. The surface temperature is set as 500 K as measured during the BSUV-2 flight.

For the problem of interest, the Knudsen number ranges from 0.01 to 1. In this range of Knudsen number, the validity of Navier-Stokes equation is in question. Hence, the BSUV-2 experiment serves as a good test case to examine where the continuum assumption breaks down.

The Navier-Stokes solver being used is an in-house built code named Hypersonics PACkage (HyPAC). HyPAC solves three-dimensional Navier-Stokes equations extended for thermal and chemical non-equilibrium flow. The equations are discretized on structured multi-block grid by using finite-volume method. Shock-capturing upwind scheme is applied for inviscid flux, and MUSCL-TVD extrapolation is used to improve the scheme to third order accurate. Second-order central difference is used for viscous flux. Both the inviscid and viscous fluxes and the source terms are evaluated in full-implicit fashion. The resulted sparse-matrices system is solved by the preconditioned GMRES method by using PETSc [12] numerical package. Translational, rotational and vibrational-electronic energy equations are solved.

For DSMC, the challenge is to calculate trace species, e.g. OH ground and electronically and vibrationally excited states. For the flow conditions considered in this study, because the number density of OH electronically and vibrationally excited states are 3 to 5 orders of magnitude lower than the number density of OH ground state, the trace species separation (TSS) algorithm [13] is implemented twice to resolve this issue, the first time for OH ground state, and the second for OH electronically and vibrationally excited states. The basic idea of TSS is to decouple the primary and trace species, and to calculate them separately using the DSMC method. Such treatment is the same as the DSMC overlay techniques [14-16]. The different place of TSS mainly lies in the generation of simulated particles of trace species. For example, at each time steps Δt, the number of hydroxyl generated in cell j

$$N_{OH,j} = \left(k_f n_{O_2,j} n_{H,j} - k_b n_{OH,j} n_{O,j} \right) \Delta V_j \Delta t / \gamma_t \quad , \tag{1}$$

where k_f and k_b are forward and backward reaction rate coefficients respectively, $n_{i,j}$ the number density of species i $\left(i = O_2, O, H, OH \right)$, ΔV_j the volume of cell j, and γ_t the ratio real-to-simulated particles of trace species. It should be noted that the number densities of primary species are obtained through a sampling and averaging in the first round of the TSS algorithm, while the number densities of trace species are updated each time step in the second round of TSS until they reach a steady state. More details see [17].

NONEQUILIBRIUM RADIATION MODEL

Due to rarefied gas effect, the electronic and vibrational states of the OH molecules do not satisfy Boltzmann distribution. Therefore, the electronic and vibrational states populations need to be computed by the flow solvers directly.

The population at state (e, v, J)

$$\mathrm{N_{evJ}} = \mathrm{N_{ev}} \frac{\mathrm{Q_J}}{\mathrm{Q_m^J}} \tag{2}$$

with

$$\mathrm{Q_m^J} = \sum_{\mathrm{J}} \mathrm{Q_J}, \tag{3}$$

where $\mathrm{N_{evJ}}$ is the number density of state (e, v, J), $\mathrm{N_{ev}}$ the summation over rotational state J, $\mathrm{Q_J}$ is the partition function of rotational state J.

The spectral emission power density is computed by

$$\mathrm{E_\lambda} = \mathrm{N_{evJ}} \mathrm{A_{ul}} \Delta \mathrm{E_{ul}} \varphi_\lambda / 4\pi, \tag{4}$$

where $\mathrm{A_{ul}}$ is the Einstein coefficient between the upper and lower state, $\Delta \mathrm{E_{ul}}$ the energy of the emitted photon, φ_λ the line shape function that assumes a Voigt line shape function [18].

TABLE 2. Four pairs overlapping rotational line braches.

Q_2	Q1	P2	R1
$^{Q}R_{12}$	$^{Q}P_{21}$	$^{P}Q_{12}$	$^{R}Q_{21}$

For band OH $A^2\sum^+ \rightarrow X^2\prod$, all the 12 branches of rotational lines are considered. However, due to the way of evaluating the rotational energy level, four pairs of rotational lines overlap that are shown in Table 2. The Franck-Condon factor, the Honl-London factor and electronic transition moment are taken from [18-20].

RESULTS AND DISCUSSION

The computed results under the experimental conditions of BSUV-2 obtained by the DSMC and Navier-Stokes methods are shown below.

Figure 2 plots the computed results along the stagnation line of BSUV-2 at altitude 80km. The temperature profiles show that flow is highly non-equilibrium, where the translational temperature is significantly higher than the rotational and vibrational-electronic temperature. At this altitude, the temperature and number density profiles obtained by Navier-Stokes are similar to those by DSMC, which indicates that the continuum assumption works at this flow condition. Note that since no-slip isothermal wall boundary condition is used in the Navier-Stokes calculation, the excited OH number density decreases near the body.

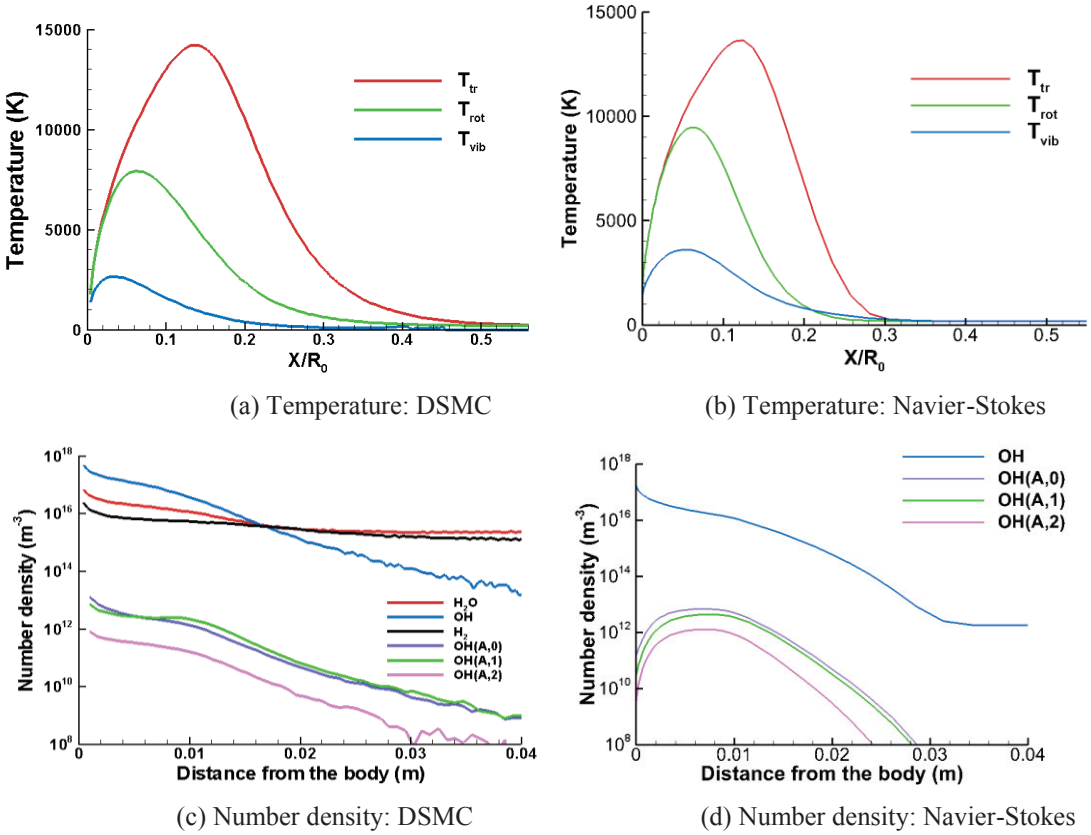

(a) Temperature: DSMC

(b) Temperature: Navier-Stokes

(c) Number density: DSMC

(d) Number density: Navier-Stokes

FIGURE 2. Computed results along the stagnation line under the experimental condition of BSUV-2 at altitude 80 km.

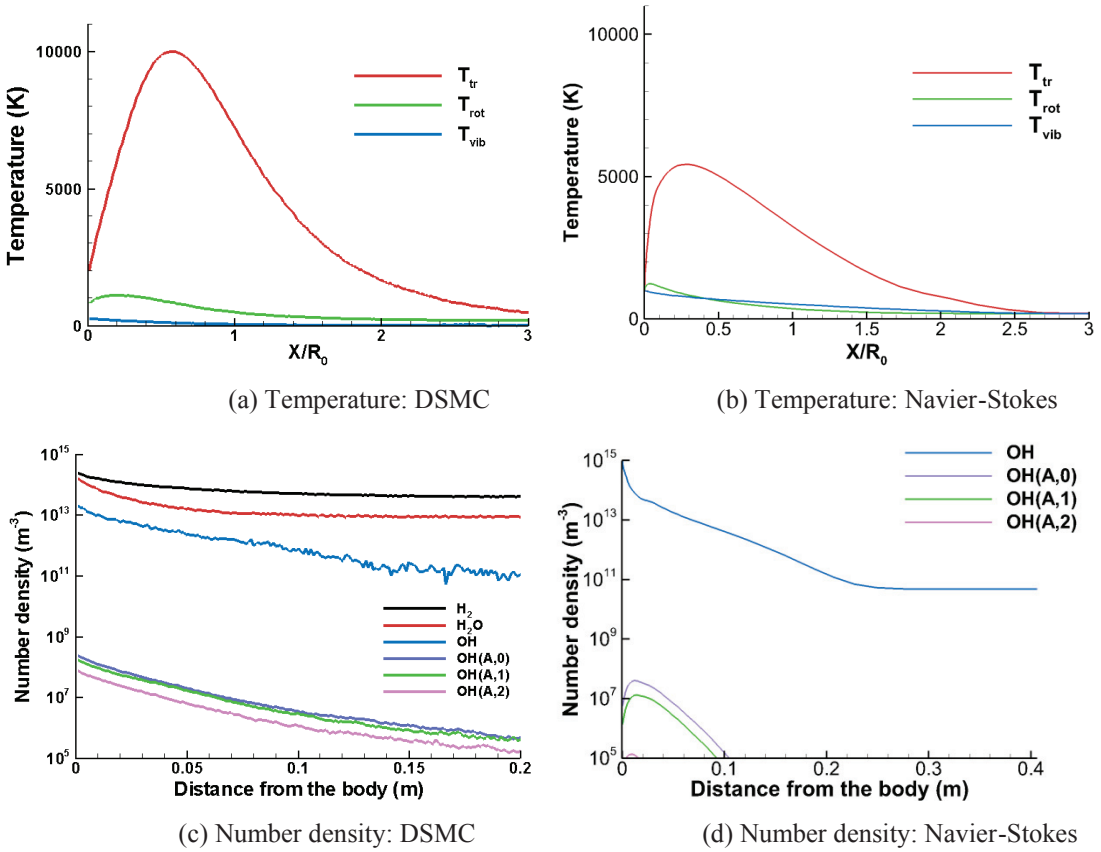

FIGURE 3. Computed results along the stagnation line under the experimental condition of BSUV-2 at altitude 100 km.

Figure 3 plots the computed results the stagnation line at 100km altitude. At this altitude, the non-equilibrium effect becomes more pronounced, and the translational temperature is significantly higher than the rotational and vibrational temperatures. The translational temperature profiles obtained by Navier-Stokes are much lower than those by DSMC, which shows that continuum assumption breaks down here. As the result of the lower temperatures, the number densities of the vibrational excited states of OH computed by Navier-Stokes are lower than those by DSMC.

Figure 4 plots the spectral radiance at the stagnation point. The "tangent-slab" method [21] is used to integrate the radiance along the stagnation line. From the spectral radiance distribution, contribution of the different vibrational bands can be observed clearly: the most significant peak is from (0, 0), (1, 1) and (2, 2) vibrational bands, and the peak existed between 280 nm and 310 nm is from (1, 0), (2, 1) and (3, 2) vibrational bands.

Figure 5 presents the spectra of OH computed by DSMC at altitude 100km, which shows a good agreement with the measured data reported in [3]. This result validates our computation of the OH spectra.

Figure 6 compares the measured and computed OH radiance of BSUV-2 at different altitudes. At 80 km and 88 km altitudes, the DSMC method shows excellent agreement with the measurement. At higher altitude, the computation is a little lower than the measurement but is still in reasonably good agreement. The Navier-Stokes results give more error than DSMC, this is because radiation is very sensitive to the temperatures, especially the vibrational-electronic temperature, at the range of altitudes, and the computation of the temperatures by Navier-Stokes has larger uncertainty. At 100 km, Navier-Stokes equation breaks down, when Navier-Stokes solver under-predicts the temperatures and the number densities of OH excited states, and hence the OH radiance.

To examine the contribution of different species to the total radiance, we switch on and off the corresponding chemical reactions. For example, in order to compute the radiance that is caused by reactions of species H_2O only, the reactions 1, 2 and 3 in Table 1 are left on, whereas the reactions 4, 5, and 6 are turned off. The ratio of the radiance so obtained to the total radiance is plotted in Fig. 7. It is found that at 80km altitude, H_2O is the most

dominating source of species OH and hence the radiance. Similarly, at 100 km altitude, atomic hydrogen is found to be the most pronounced species and the most dominating source of OH. These computed results confirm the analysis in the first two sections, i.e. at altitudes 80 km and 100 km, the most important species for OH emission are H_2O and H, respectively.

CONCLUSIONS

In this paper, four key issues of ultraviolet radiation of OH at high altitudes are discussed. The results of a typical atmospheric model were analyzed, which showed different source of H-element at different altitudes. According to that, three zones of atmosphere were defined. Important species and reaction were analyzed in the different zones. Particle (TSS) and continuum method were applied to simulate BSUV-2 flight flow field. TSS method performed well, whereas the continuum method under-predicted the temperatures at 100 km. The computed spectra were compared with the flight data, and good agreement was obtained, and so was the spectra peaks at different altitudes. Contribution of different species was computed, which confirmed our previous analysis: at 80 km and 100 km, H_2O and H were the most important species for OH emission, respectively.

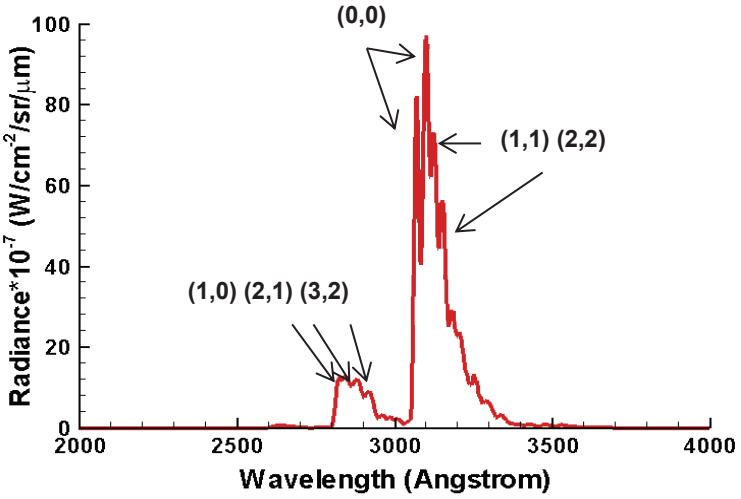

(a) 80 km

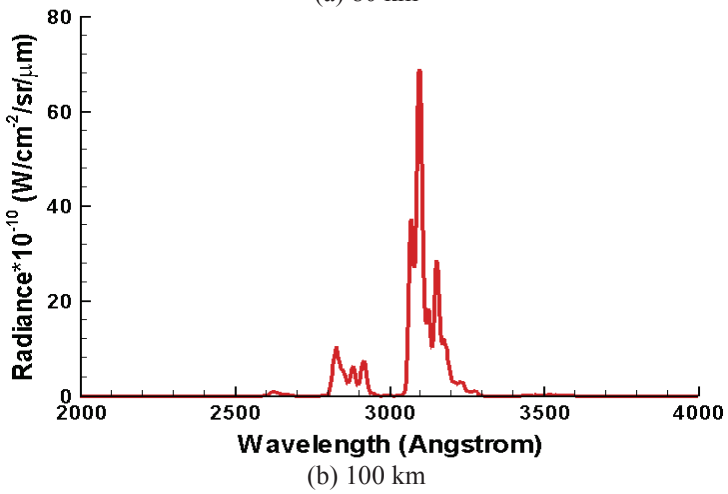

(b) 100 km

FIGURE 4. Spectral radiance at the stagnation point at (a) 80 km and (b) 100 km altitudes.

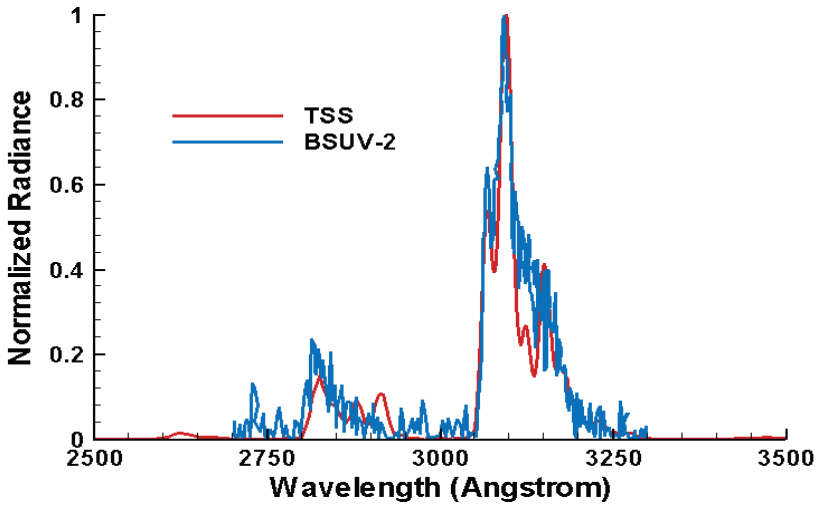

FIGURE 5. Comparison of computed and measured spectra of OH at altitude 100 km.

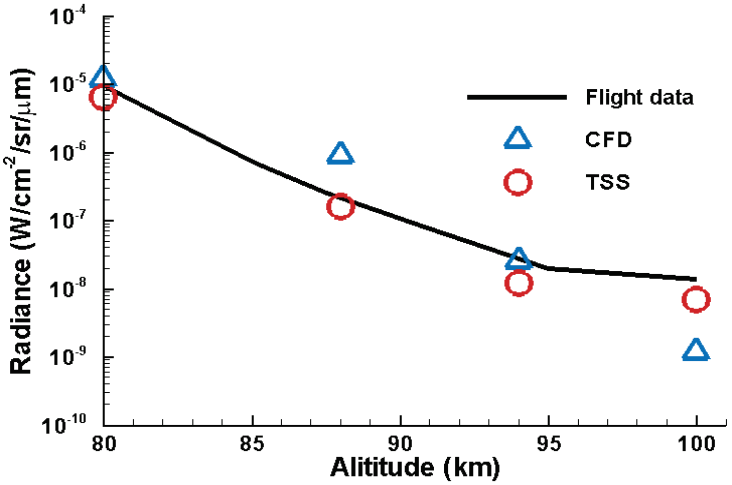

FIGURE 6. Comparison of the computed and measured OH radiances of BSUV-2 at different altitudes.

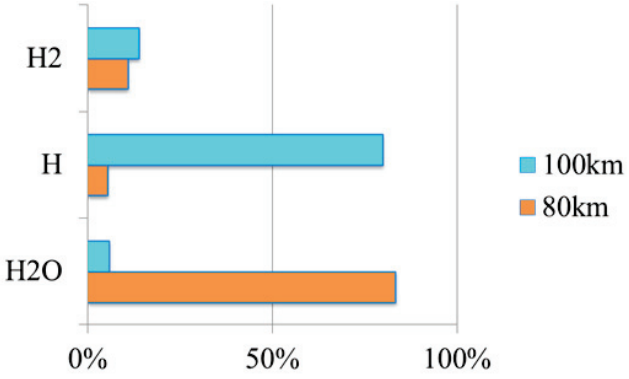

FIGURE 7. Contribution of different species to the radiance peak at altitudes 80 km and 100 km.

REFERENCES

1. P. W. Erdman, E. C. Zipf, P. J. Espy, C. Hewlett, D. A. Levin, R. Loda, R. J. Collins, and G. V. Candler, *Journal of Thermophysics and Heat Transfer* **7**, 37-41 (1993).
2. P. W. Erdman, E. C. Zipf, P. Espy, L. C. Howlett, D. A. Levin, R. J. Collins, and G. V. Candler, *Journal of Thermophysics and Heat Transfer* **8**, 441-446 (1994).
3. D. A. Levin, G. V. Candler, R. J. Collins, P. W. Erdman, E. C. Zipf, P. J. Espy, L. C. Hewlett, *Journal of Thermophysics and Heat Transfer* **8**, 447-452 (1994).
4. I. D. Boyd, W. D. Phillips and D. A. Levin, *Journal of Thermophysics and Heat Transfer* **12**, 38-44 (1998).
5. K. K. Kossi and I. D. Boyd, *Journal of Spacecraft and Rockets* **35**, 653-659 (1998).
6. K. K. Kossi, I. D. Boyd, and D. A. Levin, *Journal of Thermophysics and Heat Transfer* **12**, 223-229 (1998).
7. G. Brasseur and S. Solomon, *Aeronomy of the middle atmosphere: chemistry and physics of the stratosphere and mesosphere*, Springer, 2005.
8. N. E. Gimelshein, D. A. Levin, and S. F. Gimelshein, *AIAA Journal* **41**, 1323-1331 (2003).
9. O. P. Shatalov, L. B. Ibraquimova, V. A. Pavlov, G. D. Smekhov, and Yu. V. Tunik, "Analysis of the Kinetic Data Described Oxygen-Hydrogen Mixtures Combustion" in *4th European Combustion Meeting*, 2009, pp. 222-227.
10. M. H. Bortner, "Suggested Standard Chemical Kinetics for Flow-Field Calculations—A Consensus Opinion" in *AMRAC Proceedings*14, Inst. of Science and Technology, Univ. of Michigan, Ann Arbor, MI, 1966, pp. 569–581.
11. Bird, G.A. *Molecular Gas Dynamics and the Direct Simulation of Gas Flows*. Oxford University Press, Incorporated, 1994.
12. S. Balay, S. Abhyankar, and M. F. Adams, PETSc web page, http://www.mcs.anl.gov/petsc (2014).
13. J. Fan, Y. H. Zhang, and J. Z. Jiang (2012) CSTAM 2012-B03-0174.
14. K. P. Karipides, I. D. Boyd, and G. E. Caledonia, *Journal of Thermophysics and Heat Transfer* **12**, 30-37 (1998).
15. V. K. Dogra, R. J. Collins, and D. A. Levin, *AIAA Journal* **37**, 443-452 (1999).
16. S. F. Gimelshein, D. A. Levin, and R. J. Collins, *Journal of Thermophysics and Heat Transfer* **14**, 471-479 (2000).
17. J. Fan, Y. H. Zhang, and J. Z. Jiang, "Monte Carlo Modeling of Electron Density Distribution in Hypersonic Rarefied Gas Flows", presented at the *29th International Symposium on Rarefied Gas Dynamics*, July 13-18, 2014, Xian, China.
18. J. O. Arnold, E. E. Whiting, and G. C. Lyle, *J. Quant. Spectrosc. Radiat. Transfer* **9**, 775-798 (1969).
19. J. Luque and D. R. Crosley, *J. Chem. Phys* **109**, 439-448 (1998).
20. D. A. Levin, C. Laux, and C. H. Kruger, *J. Quant. Spectrosc. Radiat. Transfer* **61**, 377-392 (1998).
21. M. Stephane, "Computation of high-altitude hypersonic flow-field radiation", Ph. D. Thesis, Stanford University, 1994.